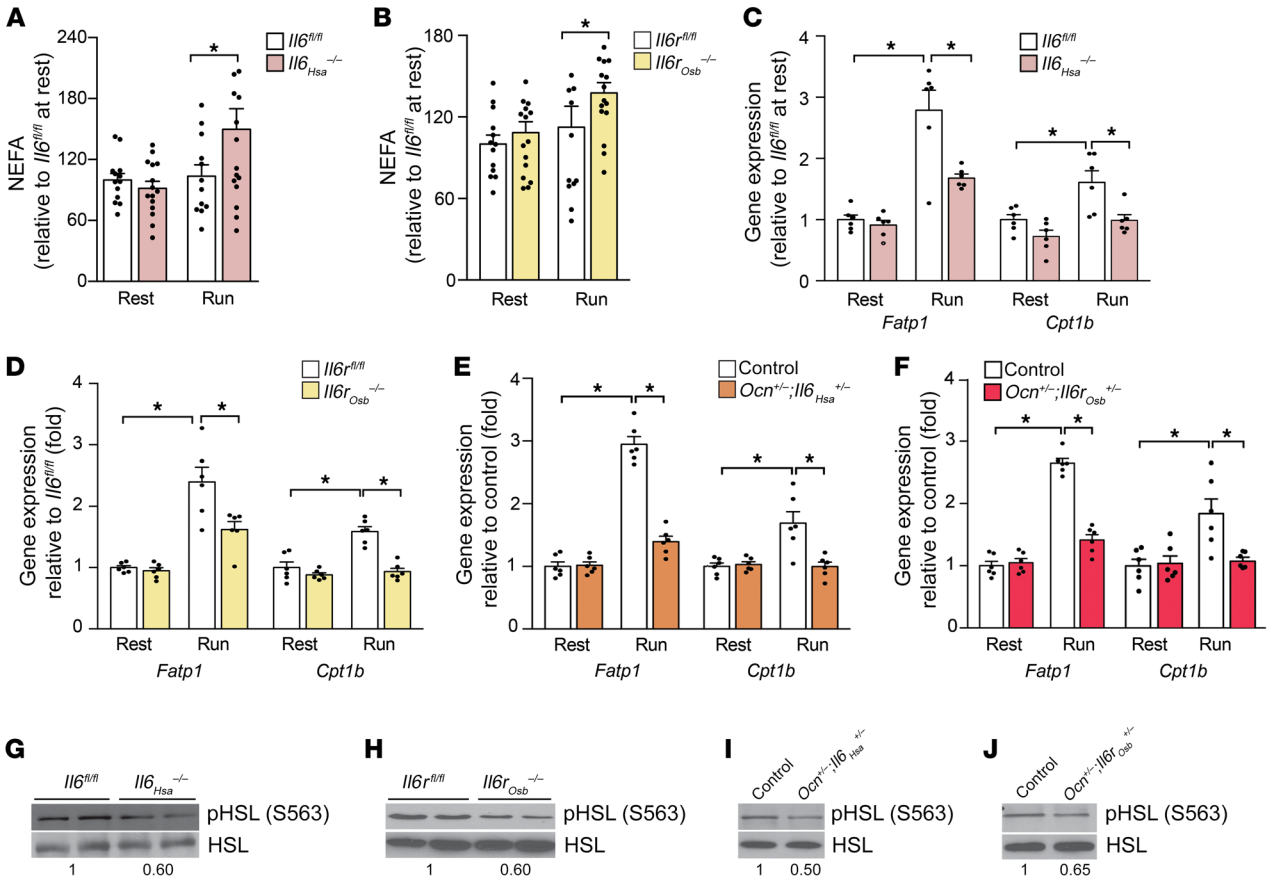

Figure 9. mIL-6 favors fatty acid uptake and catabolism in myofibers during exercise through osteocalcin. (**A** and **B**) Circulating NEFA levels at rest and after exercise in 3-month-old *Il6*$_{Hsa}^{-/-}$ and *Il6r*$_{Osb}^{-/-}$ mice and their respective controls. (**C**–**F**) Expression of *Fatp1* and *Cpt1b* at rest and after exercise in gastrocnemius of 3-month-old (**C**) *Il6*$^{fl/fl}$ and *Il6*$_{Hsa}^{-/-}$ mice, (**D**) *Il6r*$^{fl/fl}$ versus *Il6r*$_{Osb}^{-/-}$ mice, (**E**) controls (WT, *Il6*$_{Hsa}^{+/-}$, and *Ocn*$^{+/-}$) versus *Ocn*$^{+/-}$ *Il6*$_{Hsa}^{+/-}$ mice, and (**F**) controls (WT, *Il6r*$_{Osb}^{+/-}$, and *Ocn*$^{+/-}$) versus *Ocn*$^{+/-}$ *Il6r*$_{Osb}^{+/-}$ mice. (**G**–**J**) Western blot analysis of HSL phosphorylation (Ser563) in tibialis muscles of 3-month-old (**G**) *Il6*$^{fl/fl}$ versus *Il6*$_{Hsa}^{-/-}$, (**H**) *Il6r*$^{fl/fl}$ versus *Il6r*$_{Osb}^{-/-}$, (**I**) controls (WT, *Il6*$_{Hsa}^{+/-}$, and *Ocn*$^{+/-}$) versus *Ocn*$^{+/-}$ *Il6*$_{Hsa}^{+/-}$, and (**J**) controls (WT, *Il6r*$_{Osb}^{+/-}$, and *Ocn*$^{+/-}$) versus *Ocn*$^{+/-}$ *Il6r*$_{Osb}^{+/-}$ mice after exercise. These results are representative of 3 independent experiments. Data in **A**–**E** were analyzed by 1-way ANOVA followed by Tukey's post hoc test. Results presented as the mean ± SEM. *$P < 0.05$.

arm of this cross-regulation occurs first. Although this is a difficult question to address in vivo, the fact that osteocalcin acts directly on myofibers to upregulate *Il6* expression, whereas IL-6 needs to trigger a multistep pathway involving gene expression in osteoblasts, osteoclast differentiation, and eventually release bioactive osteocalcin, suggests that the bone-to-muscle arm of this crosstalk is what initiates it.

The muscle-to-bone-to-muscle pathway favoring exercise capacity described here (Figure 10) complements the previously described bone-to-muscle pathway that is also necessary to increase exercise capacity (13). Together, these 2 studies propose a new perspective on how exercise capacity is regulated by distinguishing between muscle mass and muscle function and by identifying bone via the hormone osteocalcin as a focal regulator of exercise capacity. They also provide credence to the recently proposed notion that bone might have evolved as a tool to escape danger (27).

Going forward, 2 questions will need to be addressed. First, could osteocalcin signaling in myofibers be harnessed to reverse the course of sarcopenia in clinically relevant animal models of this disease? In the long run these experiments may pave the way to harness osteocalcin signaling in muscle in order to improve muscle function in sarcopenic patients. Second, if osteocalcin emerges as a central regulator of exercise capacity it may also signal in other organs implicated in this process.

Methods

Primate studies. Adult female rhesus monkeys (*Macaca mulatta*) weighing 7 to 10 kg were individually housed in standard primate cages at the large animal facility, National Institute of Immunology, New Delhi, India. During the experimentation period, the animal rooms received continuous fresh 5-μm-filtered air ranging from 22°C–28°C and 17°C–21°C, maximum and minimum, respectively. Monkeys were injected at 1000 hours with recombinant human osteocalcin at the dose of 13.5 ng/g and blood samples were obtained by femoral venipuncture in Vacutainer blood collection tubes at different time points after injection. Blood was allowed to collect at room temperature, and serum was collected after centrifugation in aliquots and stored at –80°C until analyzed.

Mouse studies. *Il6*$^{fl/fl}$ and *HSA-*$_{MerCreMer}$ (*HSA-*$_{MCM}$) mice (Jackson Laboratory) were on the C57BL/6 genetic background. *Ocn*$^{-/-}$ mice were maintained on the 129-Sv genetic background. *Il6r*$_{Osb}^{-/-}$, *Il6r*$_{Hsa}^{-/-}$, and *Il6*$_{Hsa}^{+/-}$ *Ocn*$^{+/-}$ mice were maintained on the 129-Sv/C57BL/6 mixed

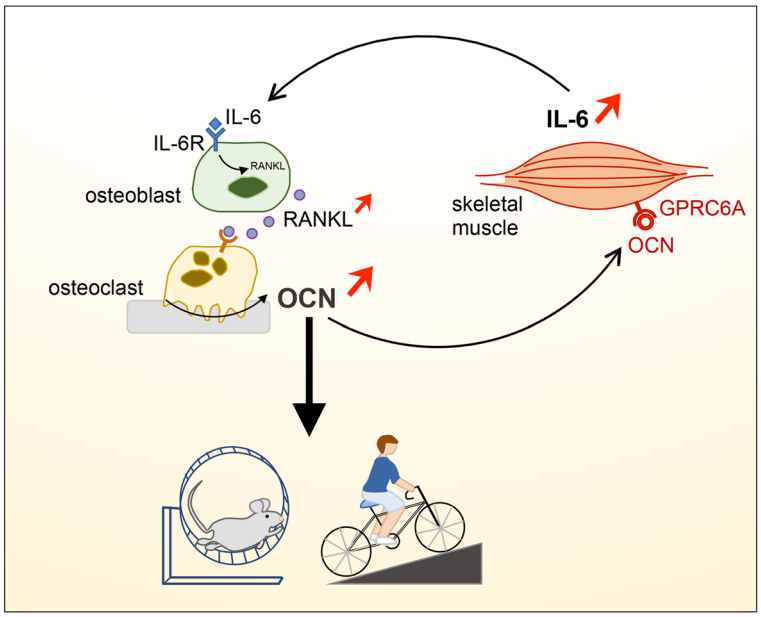

Figure 10. Schematic representation of how muscle-derived IL-6 increases exercise capacity in an osteocalcin-dependent manner.

background. To minimize the confounding effect of a different genetic background, all experiments were performed using control littermates.

Mouse genotypes were determined by PCR. For osteocalcin treatment studies, *Il6*$_{Hsa}^{-/-}$ and *Il6r*$_{Osb}^{-/-}$ mice together with their controls were implanted with subcutaneous osmotic pumps (Alzet, model 1004) delivering osteocalcin (120 ng/h) for 28 days. After this period, mice were euthanized and muscles were dissected for analyses of muscle mass. Recombinant osteocalcin was purified as previously described (28).

Exercise. For exercise studies, all mice were trained to run on a treadmill for 4 days (17 min/day, with increasing speed from 10 to 30 cm/s, and an electric shock at 0.4 mA to trigger running). Exercise tests were performed on mice fed ad libitum at 1–6 pm. On the test day, mice were acclimated to the treadmill for 5 minutes, followed by 10 minutes of running at a constant speed (17 cm/s), followed by a gradual speed increase to 30 cm/s. Mice ran either until exhaustion to determine endurance capacity, or for 40 minutes. Mice were removed from the electric grid if the number of times a mouse fell off the grid during 1 minute reached 15 or more. For all biochemical and metabolic analyses, blood/tissues were collected and processed either at rest or at the end of a 40-minute run (30 cm/s). Injections (i.p.) of exogenous osteocalcin or IL-6 (Sigma-Aldrich, I9646) were performed immediately before exercise.

Biochemistry and molecular biology. Glucose and insulin tolerance tests were performed as described previously (29). Serum osteocalcin, IL-6, and glucagon levels were measured using ELISAs. Blood glucose level was measured using an Accu-Chek glucometer.

Circulatory IL-6 levels were detected using Abcam System ELISA kits in the serum of human (Abcam, ab178013), monkey (Abcam, ab119549), rat (Abcam, ab100772), and mouse (Abcam, ab100712) according to the manufacturer's instructions. Blood was collected from the facial vein before and after exercise into tubes followed by centrifugation at 3000 *g* for 10 minutes at 4°C and serum aliquots were stored at –80°C for further use. Mouse circulating osteocalcin levels were determined with a previously described ELISA (14). Total levels of osteocalcin and carboxylated osteocalcin were estimated using 2 different specific antibodies. Bioactive osteocalcin was determined by subtracting the carboxylated osteocalcin levels from total osteocalcin levels. CTX1 (Immunodiagnostic Systems [IDS], AC-06F1) and PiNP (IDS, AC-33F1) were also measured according to the manufacturer's instructions.

Circulating level of NEFAs, triglycerides, and glycerol were determined in serum using a colorimetric triglyceride assay kit (Biovision Inc., K622-100) and glycerol assay kit (Sigma-Aldrich, MAK117) according to the manufacturers' protocols.

Gene expression analysis by qRT-PCR. Muscles and other organs were snap-frozen in liquid nitrogen and kept at –80°C until use. RNA was isolated using TRIzol (Invitrogen). RNA was first incubated with DNase I for 30 minutes at room temperature to remove any genomic DNA. DNase I–treated RNA was converted to cDNA by using M-MLV reverse transcriptase (Thermo Fisher Scientific, 28025013) and random hexamers (Thermo Fisher Scientific, N8080127). For gene expression, 1 mg of RNA was reverse transcribed into cDNA. qPCR analyses were performed using PowerUp SYBER Green Master Mix (Applied Biosciences, Thermo Fisher Scientific). SYBR Green PCR conditions were 1 cycle of 50°C for 2 minutes, 1 cycle of 95°C for 10 minutes, and 40 cycles of 95°C for 15 seconds and 60°C for 60 seconds, using a model CFX96 Touch Real-Time PCR Detection System (Bio-Rad). Relative gene expression levels were calculated using the threshold cycle ($2^{-\Delta\Delta CT}$) method and normalized to *Hprt*.

Protein expression analysis by Western blot. Lysates were prepared from skeletal muscles using modified RIPA buffer (150 mM NaCl, 1 mM EDTA, 1% Triton X-100, 1% sodium deoxycholate, 0.1% SDS, and 20 mM Tris, pH 8.0) with protease inhibitors and 1 mM sodium orthovanadate with protease inhibitor cocktail (Thermo Fisher Scientific, 862209) and homogenized before quantification by BCA assay (Thermo Fisher Scientific, 23225). After adjustment of the concentration (100 μg/100 μL) in each of the samples, equal amounts of total protein (20 μg) and SDS-Sample Buffer (Boston BioProducts, BP-110R) were boiled for 5 minutes at 98°C, and recovered by spinning at 12,000 *g* for 5 minutes at 4°C before being loaded onto a 10% or 15% SDS-PAGE gel. The gel was run for 80 minutes at 120 V in SDS-Running Buffer (Boston BioProducts, BP-177) before being transferred to a nitrocellulose membrane (Bio-Rad, 1620112) overnight at 25 V. Blots were blocked in 5% BSA (AppliChem, A0830) in Tris-buffered saline (TBS) with 0.1% Tween for 1 hour before being incubated overnight in antibodies recognizing phospho HSL (Cell Signaling Technology, 4137S, 1:1000), HSL (Cell Signaling Technology, 4107, 1:1000), or GAPDH (Cell Signaling Technology, 5174S, 1:1000). Membranes were washed with TBST (137 mM NaCl, 2.7 mM KCl, 16.5 mM Tris, pH 7.4, containing 0.1% Tween 20) before being incubated with rabbit (Santa Cruz Biotechnology, SC-2004) secondary HRP-conjugated antibodies before being imaged using ECL substrate (Bio-Rad, 170-5061) on an ImageQuant LAS-4000 (GE Healthcare, 28-9607-59AB). Band intensities were quantified using ImageJ software (NIH).

In vivo glucose uptake. A modification of a previously described method (30) was used for in vivo glucose uptake. Before exercise, mice were injected with 10 μCi of ^{3}H-2-DG in 100 μL of 0.9% NaCl.

Next, mice were placed on a treadmill and forced to run for 40 minutes at a constant speed (30 cm/s). After exercise, blood and quadriceps muscles were collected to determine ^{3}H radioactivity. ^{3}H radioactivity in blood was similar in all mice, indicating similar systemic delivery of the tracer. White and red quadriceps muscles were homogenized in 1 mL of water immediately followed by boiling for 10 minutes. After that, homogenates were spun at max speed for 10 minutes. Fifty microliters of the supernatant was added to 450 μL of water and counted in 5 mL of scintillation liquid. Nine hundred microliters were passed through an anion-exchange column (AG 1-X8 resin, Bio-Rad) to remove ^{3}H-2-DG-6-phosphate. The column was washed with 6 mL of water and 500 μL of the eluted volume was counted in 5 mL of scintillation liquid. The difference between the total and eluted ^{3}H radioactivity represents ^{3}H-2-DG-6-phosphate accumulated in the tissue.

Recombinant osteocalcin. Mouse uncarboxylated osteocalcin was purified from *E. coli* BL21 transformed with pGEX2TK-mOCN, as described previously (13, 29). Briefly, GST-osteocalcin fusion protein was produced in BL21 pLyS transformed with pGEX2TK-mOCN after induction with IPTG. Cells were collected in lysis buffer (1× PBS, 10 mM Tris pH 7.2, 2 mM EDTA, 1% Triton X-100, and 1× protease and phosphatase inhibitor cocktail [Thermo Fisher Scientific, 78443]). Following 4 freeze/thaw cycles and sonication, lysates were cleared by centrifugation. The supernatant was incubated with glutathione–Sepharose 4B (GE, 17075601) for 4 hours at 4°C. Following 6 washes with washing buffer (1× PBS, 1%Triton X-100) and 1× PBS, osteocalcin was then cleaved from the GST moiety by using thrombin (GE, 27-0846-01). Four fractions were collected and each of them was incubated with benzamidine-Sepharose (GE, 17-5123-10) for 30 minutes at room temperature to remove thrombin.

Osteoblast/osteoclast coculture. Osteoblasts were obtained from 3- to 5-day-old mice using digestion medium containing αMEM, 1.5 mg/mL collagenase P, and 2.5% trypsin/EDTA. The cells were plated in 6- or 24-well plates in αMEM with FBS (not heat inactivated) and cultured for 48 to 60 hours until confluent. For adenovirus infection, 50,000 to 75,000 cells/well (24-well plate) were plated and infection was performed the next day. Cultures were kept in the αMEM with 10% FBS until they reached confluence.

When osteoblast cultures were confluent we prepared the bone marrow cells from tibias and femurs of 4- to 10-week-old mice. Extremities of each bone were cut with scissors before flushing the bone marrow into a 15-mL Falcon tube using a 10-mL syringe connected to a 25-G 5/8-in. needle. The cell suspension was homogenized by gentle pipetting and washed twice with αMEM and resuspended in 5 mL media. The cells were counted with a hemacytometer and plated in αMEM for the desired density of 0.3×10^6 to 3×10^6 cells/well. The medium was supplemented with serum from *Il6*-null mice (10%) and supplemented with PGE2 (1×10^{-6} M) and vitamin D3 (1×10^{-6} M) to promote RankL and M-CSF expression by osteoblasts, leading to osteoclast formation. IL-6 (10 ng/mL) and sIL-6R (100 ng/mL) were added (21, 31). Half of the medium was changed every 2 days with extreme care not to aspirate the myeloid progenitor cells sitting on the osteoblasts. After coculturing for the next 5 to 8 days, the osteoblast layer was removed by washing 2 times with 1× PBS and then adding 500 μL of prewarmed digestion medium (αMEM + 0.1% collagenase + 0.2% Dispase) at 37°C for 5 to 15 minutes by carefully monitoring if osteoblasts were detaching and removing the osteoblast layer completely. Once osteoblasts were detached, osteoclasts were washed again twice with 1× PBS and fixed with paraformaldehyde (PFA) or formalin for TRAP assay or lysed in TRIzol for RNA expression analysis.

Adenoviral transduction of primary osteoblasts and bone marrow–derived osteoclast precursor cells. Adenoviral vector with the cytomegalovirus (CMV) promoter (Ad5CMVEmpty) that expresses no protein and adenoviral vector with CMV driving the expression of Cre recombinase (Ad5CMVCRE) with a titer of 1×10^{10} PFU/mL were purchased from the University of Iowa Viral Vector Core. Mouse osteoblasts and bone marrow–derived osteoclast precursor cells were transduced the day after they were plated into multiwell tissue culture plates with cell culture grade poly-L-lysine (PLL) (Sigma-Aldrich, 0.5 μL/mL). Serum-free αMEM was prepared at 50% of the typical well cell culture volume (0.5 mL/well of a 12-well plate). PLL was added just before addition of virus (MOI 200) and was allowed to incubate for 10 minutes at room temperature. The virus-containing medium was used to replace the culture medium and cells were returned to the incubator. After a transduction period of 12 hours, the viral medium was discarded and replaced with fresh complete medium (32).

Osteocalcin and IL-6 injections. For all biochemical and metabolic analyses, blood and tissues were collected and processed either at rest or at the end of a 50-minute run (30 cm/s). Injections (i.p.) of osteocalcin or IL-6 (MilliporeSigma) were performed immediately before exercise. To neutralize IL-6, 500 mg of a neutralizing antibody (R&D Systems, MAB206) (33) was administered i.p. 1 hour before exercise.

Immunohistochemistry. A whole-body transcardial perfusion was done with saline followed by fresh 4% PFA. Skeletal muscle was dissected with as little force tension manipulation as possible to maintain the overall fusiform structure to determine the axis for critical transverse embedding. The dissected muscle sample was placed in a dry weight dish for 2 to 3 minutes to allow for recovery from manipulation and then immersed in 20 volumes minimum of fresh 4% PFA for 16 to 24 hours for fixation at room temperature with agitation sufficient to move the tissue. Samples were then transfer to 1× PBS in sealed vials without any air bubbles and processed for paraffin embedding.

Muscle sections (5-μm-thick) were prepared, deparaffinized with xylene, and rehydrated with a graded series of ethanol (absolute, 95%, 90%, 80%, and 70% in water). Slides were incubated in ice-cold permeabilization solution (0.1% Triton X-100 and 0.1% sodium citrate in water) and blocked in PBS containing 10% BSA and 10% normal goat serum. Sections were stained with N0Q7 monoclonal antibody for myosin heavy chain isoform I (MHC I) slow twitch (Sigma-Aldrich, M4276) and MY32 monoclonal antibody for MHC II fast twitch (Sigma-Aldrich, M8421), followed by secondary antibody anti–mouse IgG–peroxidase and staining (Sigma-Aldrich, A8924). Images were captured with a Nikon A1 confocal microscope.

Bone histology and histomorphometry. Six-month-old $Il6r^{fl/fl}$ and $Il6r_{Osb}^{-/-}$ mice were euthanized 1 week after the last exercise. Lumbar vertebrae and tibiae from 6-month-old $Il6r^{fl/fl}$ and $Il6r_{Obs}^{-/-}$ mice were dissected, fixed in 10% buffered formalin for 24 hours, and dehydrated through a series of increasing ethanol concentrations. Samples were then embedded in methylmethacrylate (MMA) according to standard protocols. Four- and 8-μm-thick serial sections were cut and von Kossa, TRAP, and toluidine blue staining were used to measure trabecular bone volume versus tissue volume (BV/TV), osteoclast number, and osteoblast number, respectively. Bone histomorphometry analysis was performed on at least 30 fields at ×40 magnification as described previously (34) using the Osteomeasure Analysis system (Osteometrics).

Statistics. All values are depicted as mean ± SEM. Statistical parameters including the exact value of *n*, post hoc test, and statistical significance are reported in every figure and figure legends. Data were determined to be statistically significant when $P < 0.05$ by Student's *t* test or 1-way or 2-way ANOVA. Data were analyzed using GraphPad Prism 7.

Study approval. All human subjects signed a written informed consent before participating and were free to withdraw from the study at any time. The study was conducted in accordance with the guidelines for Good Clinical Practice and the Declaration of Helsinki. The study was approved by the Region Ethical Committee, Copenhagen, Denmark (H-16018062) with the registration at Clinicaltrials.gov as NCT02901496. The results have been reported in accordance with the CONSORT guidelines. All primate procedures were approved by the Institutional Animal Ethics Committee for the Care and Use of Primates in Research at the National Institute of Immunology, New Delhi, India (IAEC/2017/157). All experiments involving mice were approved by the Institutional Animal Care and Use Committee of the Columbia University Medical Center.

Author contributions

SC and GK conceived of the study and designed experiments. SC, LS, BP, PS, JMB, VKY, and PM performed experiments. HH contributed sera from patients. JH and JB provided floxed mice. SC and GK analyzed data and wrote the manuscript.

Acknowledgments

We thank Gerald Shulman (Yale University), Patricia Ducy (Columbia University), and Mathieu Ferron (Montreal Clinical Research Institute-IRCM) for advice, reagents, and reading the manuscript. This work was supported by 5R01DK104727-05 (NIDDK) (to GK), 1R01AR073180-01A1 (NIAMS) (to GK), Canadian Institute of Health and Research (CIHR) Fellowship (201511MFE-359182-181537) (to SC), Ramalingaswamy Fellowship (BT/HRD/35/02/2006), Department of Biotechnology, India (to VKY), Ministerio de Economía y Competitividad y Fondo Europeo de Desarrollo Regional SAF2014-56546-R and RTI2018-101105-B-I00 (to JH), TrygFonden (grants ID 101390 and ID 20045) (to HE).

1. Neufer PD, et al. Understanding the cellular and molecular mechanisms of physical activity-induced health benefits. *Cell Metab*. 2015;22(1):4–11.
2. Zierath JR, Wallberg-Henriksson H. Looking ahead perspective: where will the future of exercise biology take us? *Cell Metab*. 2015;22(1):25–30.
3. Pedersen BK, Febbraio MA. Muscles, exercise and obesity: skeletal muscle as a secretory organ. *Nat Rev Endocrinol*. 2012;8(8):457–65.
4. Ostrowski K, Rohde T, Zacho M, Asp S, Pedersen BK. Evidence that interleukin-6 is produced in human skeletal muscle during prolonged running. *J Physiol (Lond)*. 1998;508(pt 3):949–953.
5. Steensberg A, van Hall G, Osada T, Sacchetti M, Saltin B, Klarlund Pedersen B. Production of interleukin-6 in contracting human skeletal muscles can account for the exercise-induced increase in plasma interleukin-6. *J Physiol (Lond)*. 2000;529(pt 1):237–242.
6. Pedersen BK, et al. Searching for the exercise factor: is IL-6 a candidate? *J Muscle Res Cell Motil*. 2003;24(2–3):113–119.
7. Lang Lehrskov L, et al. Interleukin-6 delays gastric emptying in humans with direct effects on glycemic control. *Cell Metab*. 2018;27(6):1201–1211.e3.
8. Wedell-Neergaard AS, et al. Exercise-induced changes in visceral adipose tissue mass are regulated by IL-6 signaling: a randomized controlled trial. *Cell Metab*. 2019;29(4):844–855.e3.
9. Febbraio MA, Hiscock N, Sacchetti M, Fischer CP, Pedersen BK. Interleukin-6 is a novel factor mediating glucose homeostasis during skeletal muscle contraction. *Diabetes*. 2004;53(7):1643–1648.
10. van Hall G, et al. Interleukin-6 stimulates lipolysis and fat oxidation in humans. *J Clin Endocrinol Metab*. 2003;88(7):3005–3010.
11. Catoire M, Kersten S. The search for exercise factors in humans. *FASEB J*. 2015;29(5):1615–1628.
12. Hawley JA, Hargreaves M, Joyner MJ, Zierath JR. Integrative biology of exercise. *Cell*. 2014;159(4):738–749.
13. Mera P, et al. Osteocalcin signaling in myofibers is necessary and sufficient for optimum adaptation to exercise. *Cell Metab*. 2016;23(6):1078–1092.
14. Ferron M, et al. Insulin signaling in osteoblasts integrates bone remodeling and energy metabolism. *Cell*. 2010;142(2):296–308.
15. Johnson RW, et al. The primary function of gp130 signaling in osteoblasts is to maintain bone formation and strength, rather than promote osteoclast formation. *J Bone Miner Res*. 2014;29(6):1492–1505.
16. McCarthy JJ, Srikuea R, Kirby TJ, Peterson CA, Esser KA. Correction: Inducible Cre transgenic mouse strain for skeletal muscle-specific gene targeting. *Skelet Muscle*. 2012;2(1):22.
17. Miniou P, Tiziano D, Frugier T, Roblot N, Le Meur M, Melki J. Gene targeting restricted to mouse striated muscle lineage. *Nucleic Acids Res*. 1999;27(19):e27.
18. von Maltzahn J, Jones AE, Parks RJ, Rudnicki MA. Pax7 is critical for the normal function of satellite cells in adult skeletal muscle. *Proc Natl Acad Sci U S A*. 2013;110(41):16474–16479.
19. Suda T, Takahashi N, Martin TJ. Modulation of osteoclast differentiation. *Endocr Rev*. 1992;13(1):66–80.
20. Mihara M, Hashizume M, Yoshida H, Suzuki M, Shiina M. IL-6/IL-6 receptor system and its role in physiological and pathological conditions. *Clin Sci*. 2012;122(4):143–159.
21. McGregor NE, et al. IL-6 exhibits both *cis*- and *trans*-signaling in osteocytes and osteoblasts, but only *trans*-signaling promotes bone formation and osteoclastogenesis. *J Biol Chem*. 2019;294(19):7850–7863.
22. Zhang M, et al. Osteoblast-specific knockout of the insulin-like growth factor (IGF) receptor gene reveals an essential role of IGF signaling in bone matrix mineralization. *J Biol Chem*. 2002;277(46):44005–44012.
23. Wunderlich FT, et al. Interleukin-6 signaling in liver-parenchymal cells suppresses hepatic inflammation and improves systemic insulin action. *Cell Metab*. 2010;12(3):237–249.
24. Perry RJ, et al. Hepatic acetyl CoA links adipose tissue inflammation to hepatic insulin resistance and type 2 diabetes. *Cell*. 2015;160(4):745–758.
25. Stahl A, Gimeno RE, Tartaglia LA, Lodish HF. Fatty acid transport proteins: a current view of a growing family. *Trends Endocrinol Metab*. 2001;12(6):266–273.
26. Mera P, Laue K, Wei J, Berger JM, Karsenty G. Corrigendum to "Osteocalcin is necessary and sufficient to maintain muscle mass in older mice" [Mol Metabol 5 (2017) 1042–1047]. *Mol Metab*. 2017;6(8):941.
27. Berger JM, et al. Mediation of the acute stress response by the skeleton. *Cell Metab*. 2019;30(5):890–902.e8.
28. Oury F, et al. Maternal and offspring pools of osteocalcin influence brain development and functions. *Cell*. 2013;155(1):228–241.
29. Lee NK, et al. Endocrine regulation of energy metabolism by the skeleton. *Cell*. 2007;130(3):456–469.
30. Howlett KF, Andrikopoulos S, Proietto J, Hargreaves M. Exercise-induced muscle glucose uptake in mice with graded, muscle-specific GLUT-4 deletion. *Physiol Rep*. 2013;1(3):e00065.
31. Tamura T, et al. Soluble interleukin-6 receptor triggers osteoclast formation by interleukin 6. *Proc Natl Acad Sci U S A*. 1993;90(24):11924–11928.
32. Buo AM, Williams MS, Kerr JP, Stains JP. A cost-effective method to enhance adenoviral transduction of primary murine osteoblasts and bone marrow stromal cells. *Bone Res*. 2016;4:16021.
33. Pedersen L, et al. Voluntary running suppresses tumor growth through epinephrine- and IL-6-dependent NK cell mobilization and redistribution. *Cell Metab*. 2016;23(3):554–562.
34. Yadav VK, et al. Lrp5 controls bone formation by inhibiting serotonin synthesis in the duodenum. *Cell*. 2008;135(5):825–837.